Synthesis, Structure and Vibrational Spectra of $Ba_{14}InP_{11}$

Wilder Carrillo-Cabrera, Mehmet Somer, Karl Peters, and Hans Georg von Schnering*

Max-Planck-Institut für Festkörperforschung,
Heisenbergstraße 1, D-70569 Stuttgart, FRG

Received April 30, 1996

Key Words: $Ba_{14}InP_{11}$ / Zintl phase / Tetraphosphidoindate(III) anions / Asymmetric $[P_3]^{7-}$ polyanions / Interpenetrating hierarchical frameworks

$Ba_{14}InP_{11}$ was prepared from the elements in a sealed stainless steel ampoule at 1345 K. The compound is black, brittle and very sensitive to air and moisture. $Ba_{14}InP_{11}$ crystallises in the tetragonal $Ca_{14}AlSb_{11}$ type (space group $I4_1/acd$, No. 142; a = 17.097(2) Å, c = 22.940(5) Å; Z = 8, Pearson code $tI208$). The structure contains isolated P^{3-}, linear $[P_3]^{7-}$ and tetrahedral $[InP_4]^{9-}$ anions. The X-ray structure analysis and the vibrational spectra show that the $[P_3]^{7-}$ polyanion is strongly asymmetric with d(P–P) = 2.28 Å and 4.10 Å, corresponding to a $[P_2]^{4-}$ dumbbell weakly coupled to a single P^{3-} anion. The tetraphosphidoindate(III) anion $[InP_4]^{9-}$ is slightly compressed along the $\bar{4}$ axis, with bond length d(In–P) = 2.71 Å. It is shown that the structure is hierarchically related to that of Cu_2O, with two interpenetrating frameworks, in which the O and Cu atoms are replaced by condensed $[InP_{4/2}]$ tetrahedra and $[BaP_4P_{2/2}]$ octahedra, respectively. Both frameworks are *meso* configured, containing alternate *R* and *S* fragments. The other Ba cations envelop the P_6 octahedra and P_3 triads forming condensed cubes, tetragonal antiprisms and bicapped trigonal prisms. Therefore, the structure also forms a heterogeneous framework of centred $PBa^{tap}_{8/2}$ tetragonal antiprisms and $BaBa^{cub}_{8/2}$ cubes, consisting of two interpenetrating enantiomorphic nets (*R* and *S*) similar to those in the cubic phase $RhBi_4$.

1 Introduction

The $Ca_{14}AlSb_{11}$ structure type, discovered by Cordier, Schäfer and Stelter[1] is characterised by tetrahedral tetraantimonidoaluminate(III) anions and linear Sb_3 polyanions as covalently bonded units: $Ca_{14}[AlSb_4][Sb_3]Sb_4$. This compound fulfils the well-known Zintl-Klemm concept with the formal charges Ca^{2+}, Sb^{3-}, $[AlSb_4]^{9-}$ and $[Sb_3]^{7-}$, in which the linear $[Sb_3]^{7-}$ anion is isosteric with, e.g., $[I_3]^-$ [2]. Recently, a large number of chemical derivatives were synthesised[3–8], including variants containing vacancies as in the case of $Sr_{13}\square NbAs_{11}$[9]. In this compound, the asymmetry of the $[X_3]^{7-}$ anions was first recognised. A carefully analysis of the crystallographic data of all the members of this family clearly indicates a tendency for the $[X_3]^{7-}$ units to be asymmetric. Apparently, this effect is strongly related to the size of the various atoms, especially to the size of the cation cage that envelops the $[X_3]^{7-}$ triad[10]. $Ba_{14}InP_{11}$, having the largest majority cation and the smallest E15 anion, exhibits the most pronounced asymmetry of the triad so far. Reported here is the synthesis, crystal structure, Raman and IR spectra of this interesting new compound.

2 Results and Discussion

2.1 Synthesis and Properties

$Ba_{14}InP_{11}$ was prepared by direct synthesis from the elements (atomic ratios of Ba/In/P = 14/2/12) in a sealed stainless steel ampoule with an inner corundum crucible at 1345 K. In the starting nomial composition, an excess of In and P was necessary in order to get a single-phase final product. This might compensate for the losses due to partial reaction with the walls of the ampoule and prevent the formation of Ba_3P_2. Several attempts to synthesise $Ba_{14}InP_{11}$ from stoichiometric mixtures (using different heating times) did not result in single-phase products. These samples contained only small quantities of $Ba_{14}InP_{11}$ together with the majority phase Ba_3P_2. The formation of the title compound is perhaps slowed down by the stability of Ba_3P_2 (defect Th_3P_4 type, containing only discrete P^{3-} anions[11,22]). The single-crystals were obtained from a more (In/P)-rich sample prepared in a similar way (nominal composition Ba/In/P = 3/1/3). The investigation of other (In/P)-rich samples revealed the existence of the ternary phase $Ba_3In_2P_4$, which was fully characterised (space group $C2/c$; a = 13.974 Å, b = 10.869 Å, c = 7.064 Å, β = 89.73°; Pearson code $mC36$), and is isotypic to the monoclinic phase $Ca_3Al_2As_4$[12].

The optical band gap of $Ba_{14}InP_{11}$ is 1.6 eV (determined by diffuse reflection). This value is in agreement with the observed colour (black). The compound forms prismatic crystals, and is brittle, as well as very sensitive to oxygen and moisture. It hydrolyses rapidly in wet air (emanating PH_3 gas). The decomposition products have not been characterised up to now.

2.2 Crystal Structure and Bonding

The phase $Ba_{14}InP_{11}$ (isotypic to $Ca_{14}AlSb_{11}$[1]) crystallises in the space group $I4_1/acd$, with a = 17.097(2) Å and c = 22.940(5) Å, and Z = 8. The compound belongs to the Zintl phases because of the formation of polyphosphide anions. Previous descriptions of this structure type[1,3] were focused only on the covalent bonded units. Due to the complexity of the structure, several features will be described

  0009–2940/96/0909–1015 $ 15.00+.25/0

here in detail. First, we will describe the anionic partial structure, including the structural framework formed by the P atoms around Ba3 (first coordination sphere), and second, the structural framework formed by the other Ba atoms around P1, P4 and Ba3 (second coordination sphere).

The electron balance follows the Zintl-Klemm concept[13,14], which allows the transference of the valence electrons in different ways: the 31 valence electrons of the metal atoms (14 Ba^{2+} + In^{3+}) are transferred to the 11 P atoms, which are the most electronegative ones, forming 8 P^{3-} and one $[P_3]^{7-}$ anion *or* 9 P^{3-} and one $[P_2]^{4-}$ dumbbell *or* 10 P^{3-} and one P^{1-} as part of a chain or ring. Alternatively, the 28 valence electrons of the 14 Ba atoms may be transferred to the InP_4 tetrahedron as a whole to form one $[InP_4]^{9-}$ anion (corresponding to, e.g., $[InCl_4]^-$ or $SnCl_4$) and to the remaining 7 P atoms to form the different phosphide anions.

2.2.1 The Building Units of the Phosphorus Partial Structure

The anionic partial structure of $Ba_{14}InP_{11}$ (Figure 2a) consists of isolated P^{3-}, linear $[P_3]^{7-}$ units and tetrahedral $[InP_4]^{9-}$ anions. The P^{3-} anions are formed by P3 (Table 2), and the $[P_3]^{7-}$ triad is crystallographically composed by a central P4 and two P1 as *exo* atoms (both atoms are at split positions; Figure 1, section 2.2.2). The covalent $[InP_4]^{9-}$ unit (formed by In and P2; $\bar{4}$ symmetry) is slightly compressed along the $\bar{4}$ axis, showing bond angles of 107.1° (4×) and 114.2° (2×), and bond lengths d(In–P) = 2.71 Å (4×). The $[P_3]^{7-}$ unit is isoelectronic to $[Cl_3]^-$, $[Br_3]^-$ and $[I_3]^-$, and the tetrahedral $[InP_4]^{9-}$ unit is isoelectronic to $[InCl_4]^-$ and $SnCl_4$. As far as we know, the tetraphosphidoindate(III) anion has not been observed before.

2.2.2 The Shape of the $[P_3]^{7-}$ Anion

The splitting of the central P4 and of the *exo* atoms P1 (Table 2, Figure 1) indicates that the $[P_3]^{7-}$ anion is strongly asymmetric and orientationally disordered. The mean interatomic distance $\bar{d}$(P4–P1) = 3.19 Å is much smaller than the van der Waals distance of about 3.60 Å, but it is far from the typical single bond lengths observed in polyphosphides, which vary from 2.16 Å up to 2.30 Å[15] and which are strongly influenced by structural strains and by the effective charges. Due to the mean displacements of P4 (u = ±0.74 Å) and P1 (u = ±0.18 Å) from their average positions, the real interatomic distances correspond to one of the following sets (see Figure 1e):

(a) d_1(P–P) = 2.28 Å and d_2(P–P) = 4.10 Å
(b) d_1'(P–P) = 2.46 Å and d_2'(P–P) = 3.92 Å.

By using the well known Donnay-Allmann bond order relationship[16] $S_n = (^1D/d_n)^5$, and assuming a total bond order of 1, from each of the above sets of bond distances it is possible to calculate ^1D and compare these two values to known values for P–P single bonds. Thus, for the first set of proposed interatomic distances, case **(a)**, the relationship is:

$\Sigma S_n = 1 = [^1D/(2.28\ Å)]^5 + [^1D/(4.10\ Å)]^5$

Figure 1. Different stages in the structure refinement of the $[P_3]^{7-}$ triad and the final interpretation: isotropic (a) and anisotropic (b) shapes for P1 at 16*f* site and P4 at 8*b* site, intermediate (c) and final (d) split-position structures, and (e) model of the [P–P···P] arrangement according to (d) in two complementary orientations (black and white) with labelled interatomic distances (cf. Table 3). Notice the extraordinarily large displacement for P4 in (a) and (b). In (d), the P atoms lie at three 16*f* sites with normal isotropic displacements (cf. Table 2). The Ba envelope consists of one central tetragonal antiprism sharing quadrangular faces with two bicapped trigonal prisms (a total of 16 Ba atoms). ORTEP plots (75% probability)

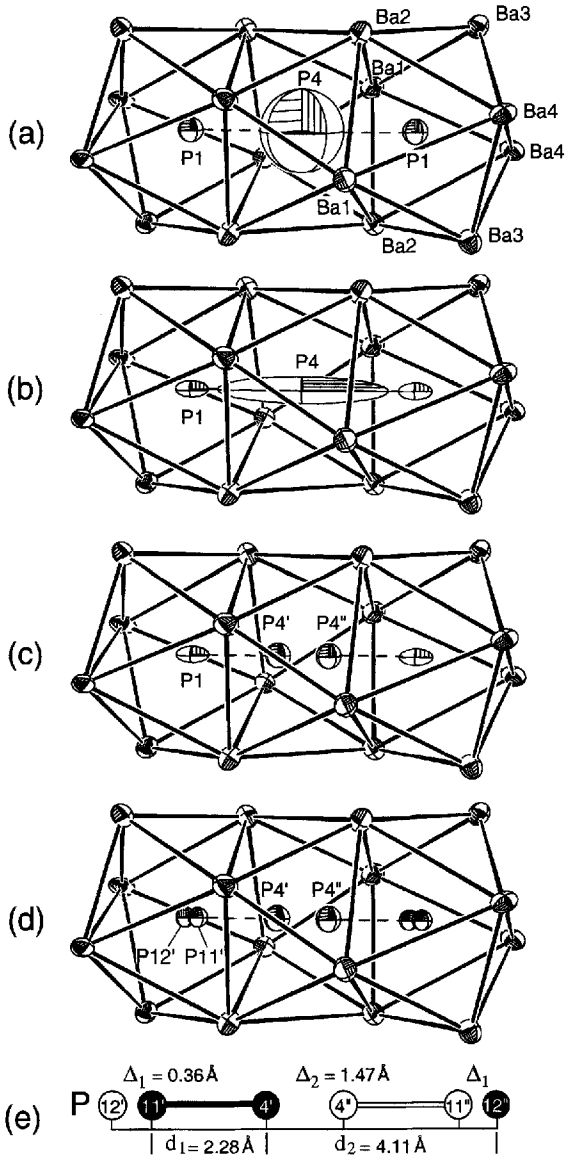

which gives ^1D(**a**) = 2.25 Å. The calculation for case **(b)** gives ^1D(**b**) = 2.41 Å. However, as we have previously stated, typical ^1D values for polyphosphides fall in the range from 2.16 Å to 2.30 Å. Therefore, for $Ba_{14}InP_{11}$, case **(a)** provides the most reasonable set of distances for the asymmetric $[P_3]^{7-}$ triad. Thus, the real shape of the $[P_3]^{7-}$ unit is a single bonded $[P_2]^{4-}$ dumbbell and one distant P^{3-} single anion, statistically disordered in two orientations as illustrated in Figure 1e (black or white). Notice that in most of the figures this group is idealised for simplicity to a sym-

Table 1. Crystallographic data

	$Ba_{14}InP_{11}$
Molar mass	2378.11 amu
Crystal characteristics	black prism (0.10 × 0.06 × 0.05 mm)
Crystal System	tetragonal
Space group; formula units	$I4_1/acd$ (No. 142); $Z = 8$
Structure type; Pearson code	$Ca_{14}AlSb_{11}$; tI_c208
Unit cell dimensions (297 K)	$a = 17.097(2)$ Å, $c = 22.940(5)$ Å $c/a = 1.3418$; $V = 6706(2)$ Å^3
d_{calc}	4.711 g·cm^{-3}
Data collection (297 K)	Siemens-Nicolet four-circle diffractometer, Mo-$K\alpha$ ($\lambda = 0.71073$ Å); ω-scan mode; $2\theta \leq 55°$
Data correction	Empirical absorption correction (ψ-scan method), $\mu = 173$ cm^{-1}, min. and max. transmission: 0.06, 0.11.
Structure refinement	SHELXTL [25]; starting set from $Ca_{14}AlSb_{11}$ 58 variable parameters
Measured/unique N(hkl)	2172 / 1900
N′(hkl) with $[F_o > 4\sigma(F_o)]$	893
Weighting	$1/(\sigma^2(F_o) + 0.0006 \cdot F_o^2$
$R(F)$; $R_w(F)$	0.080; 0.075

metric [P−P−P] linear segment (using the average positions of P1 and P4 atoms), and in the text is called the $[P_3]^{7-}$ unit or triad.

As in the case of the 22 electron systems $[I_3]^-$ and $[Br_3]^-$[2], asymmetric $[X_3]^{7-}$ (X = As, Sb) units have been observed before[9,10]. But, the $[P_3]^{7-}$ triad (properly a [P−P···P] group) in $Ba_{14}InP_{11}$ with the ratio $d_1/d_2 = 0.56$ represents an extreme case, being even more asymmetric than the $[Br_3]^-$ anion of $[PBr_4]Br_3$ ($d_1/d_2 = 0.82$[2]) or the $[As_3]^{7-}$ anion of $Sr_{13}NbAs_{11}$ ($d_1/d_2 = 0.79$[9]). In these two systems, the third atom associated with the triad is partially bonded to the central atom of the triad. However, in the case of the asymmetric $[P_3]^{7-}$ of $Ba_{14}InP_{11}$, the third P lies outside of the normal van der Waals distance of 3.60 Å. Otherwise, these d_1/d_2 ratios can be compared with those in the crystalline phases of the group 16 and group 17 elements: Cl_2 (0.61), Br_2 (0.68), I_2 (0.75) and S (0.60), Se

Figure 2. (a) Perspective view of the $Ba_{14}InP_{11}$ structure showing some building units, namely $[InP_4]$ tetrahedra (shaded), linear $[P_3]$ triads and BaP_6^{oct} octahedra (black). One Ba_8^{cub} cubic frame around one BaP_6^{oct} is also shown. (b) Same as (a) but without Ba atoms to see the distribution and orientation of the $[InP_4]^{9-}$ and $[P_3]^{7-}$ anions. One of the pseudo *bcc* unit cells contained in the structure is emphasised (shaded)

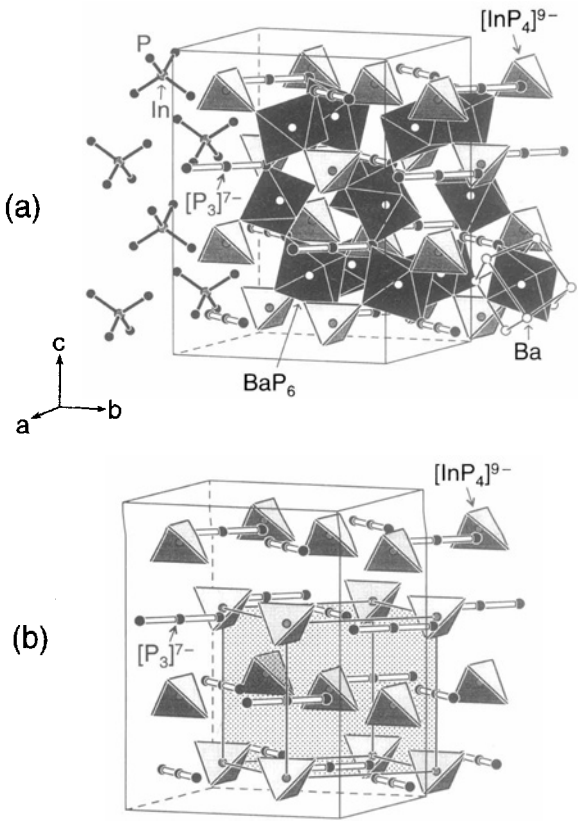

Table 2. Positional and displacement parameters (pm^2) for $Ba_{14}InP_{11}$. Space group $I4_1/acd$, No. 142 (origin at (2/*m*), 2nd choice). The displacement factor is of the form: $\exp[-2\pi^2(U_{11}h^2a^{*2} + \cdots + 2\,U_{23}klb^*c^*)]$. Standard deviations are given in parentheses. The average positions $P1_{av}$ and $P4_{av}$ are listed at the bottom

Atom	Pos.	SOF	x	y	z	U_{11}/U_{iso}	U_{22}	U_{33}	U_{12}	U_{13}	U_{23}
Ba1	32*g*	1	0.0435(1)	0.0719(2)	0.1714(1)	241(13)	381(15)	224(13)	−71(11)	46(10)	−72(12)
Ba2	32*g*	1	0.0238(1)	0.3790(1)	0.0043(1)	186(11)	223(12)	248(13)	21(9)	7(10)	−54(11)
Ba3	16*e*	1	0.3489(2)	0	1/4	234(17)	212(15)	243(17)	0	0	48(14)
Ba4	32*g*	1	0.3451(2)	0.0733(1)	0.0954(1)	407(14)	187(11)	169(11)	−3(11)	90(11)	45(10)
In1	8*a*	1	0	1/4	3/8	206(16)	U_{11}	109(24)	0	0	0
P11[a]	16*f*	0.50	0.1248(13)	$x + 1/4$	1/8	174(42)					
P12[a]	16*f*	0.50	0.1396(13)	$x + 1/4$	1/8	U(P11)					
P2	32*g*	1	0.3667(6)	0.2546(6)	0.0609(5)	253(54)	218(52)	233(54)	23(44)	−19(44)	9(45)
P3	32*g*	1	0.1312(6)	0.0267(6)	0.0456(5)	255(56)	217(52)	258(60)	−3(41)	20(46)	38(43)
P4[b]	16*f*	0.50	0.0304(14)	$x + 1/4$	1/8	290(68)					
[$P1_{av}$	16*f*		0.1321(7)	$x + 1/4$	1/8	381(54)	U_{11}	125(74)	142(72)	7(46)	$-U_{13}$]
[$P4_{av}$	8*b*		0	1/4	1/8	3205(739)					]

[a,b] Split positions of the average sites at the bottom.

Table 3. Main interatomic distances (Å) and bond angles (°) in $Ba_{14}InP_{11}$. The d(Ba-P) distances involving the split positions P11, P12 or P4 are alternative (the multiplicity is divided by two (i.e. 1/2 × or 1 × instead of 1 × or 2 ×). For P11′, P12″ and P4′ atoms, the black ordered model in Figure 1e is assumed (d_1 and d_2 distances)

Ba1	– P4′	3.02(1)	½ ×	P11′	– P4′	2.28(3)		(d_1)
	– P11′	3.20(2)	½ ×		– Ba1	3.20(2)	2 ×	
	– P3	3.28(1)			– Ba2	3.26(1)	2 ×	
	– P3	3.35(1)			– Ba4	3.50(1)	2 ×	
	– P2	3.35(1)			– Ba3	3.61(1)	2 ×	
	– P12″	3.37(2)	½ ×					
	– P2	3.39(1)		P12″	– P4′	4.11(3)		(d_2)
	– P4″	3.73(2)	½ ×		– Ba4	3.22(2)	2 ×	
					– Ba1	3.37(2)	2 ×	
Ba2	– P2	3.20(1)			– Ba2	3.41(1)	2 ×	
	– P4′	3.24(1)	½ ×		– Ba3	3.44(1)	2 ×	
	– P3	3.25(1)						
	– P11′	3.27(1)	½ ×	P2	– In1	2.71(1)		
	– P3	3.31(1)			– Ba2	3.20(1)		
	– P12″	3.41(1)	½ ×		– Ba4	3.22(1)		
	– P2	3.83(1)			– Ba1	3.35(1)		
	– P4″	3.99(2)	½ ×		– Ba1	3.39(1)		
					– Ba4	3.43(2)		
Ba3	– P3	3.12(1)	2 ×		– Ba3	3.49(1)		
	– P12″	3.44(1)	1 ×		– Ba2	3.83(1)		
	– P2	3.49(1)	2 ×					
	– P11′	3.61(2)	1 ×	P3	– Ba3	3.12(1)		
					– Ba2	3.25(1)		
Ba4	– P12″	3.22(1)	½ ×		– Ba1	3.28(1)		
	– P2	3.22(1)			– Ba2	3.31(1)		
	– P3	3.34(1)			– Ba4	3.34(1)		
	– P3	3.36(1)			– Ba1	3.35(1)		
	– P2	3.43(1)			– Ba4	3.36(2)		
	– P11′	3.50(2)	½ ×		– Ba4	3.92(2)		
	– P3	3.92(1)						
				P4′	– P11′	2.28(1)		(d_1)
					– P12″	4.11(3)		(d_2)
In1	– P2	2.71(1)	4 ×		– Ba1	3.02(1)	2 ×	
					– Ba2	3.24(1)	2 ×	
P2 – In1 – P2		107.1(2) °	4 ×		– Ba1	3.73(2)	2 ×	
P2 – In1 – P2		114.4(4) °	2 ×		– Ba2	3.99(2)	2 ×	
Ba1	– $P1_{av}$	3.28(1)		Ba4	– $P1_{av}$	3.36(1)		
	– $P4_{av}$	3.310(3)						
				P11′	– P12′	0.36(3)		(Δ_1)
Ba2	– $P1_{av}$	3.332(7)						
	– $P4_{av}$	3.563(2)		P4′	– P4″	1.47(5)		(Δ_2)
Ba3	– $P1_{av}$	3.520(7)	2 ×	$P1_{av}$	– $P4_{av}$	3.19(1)	2 ×	($\bar{d}$)

(0.69), Te (0.83), where d_2 is the distance to the next closest neighbour (namely third atom).

The presence of a single bonded $[P_2]^{4-}$ dumbbell, weakly coupled to a distant P^{3-} single anion, is confirmed by the Raman spectrum analysis (section 2.3). Therefore, the splitting of the P1 and P4 positions indeed results from the orientational disorder of the [P–P···P] arrangement, and not from dynamic transitions [P–P···P]⟺[P···P–P]. In other words, the $[P-P-P]^{7-}$ triad in $Ba_{14}InP_{11}$ is a dissociated $[P-P\cdots P]^{7-}$ unit encapsulated in a cage (Figure 1).

2.2.3 The Phosphorus Framework

A rather rough inspection of the structure of $Ba_{14}InP_{11}$ (Figure 2b) suggests that the distribution of the $[InP_4]^{9-}$ and $[P_3]^{7-}$ units (sites 8(*a*) and 8(*b*) of $I4_1/acd$) may be similar to that of the Na and Cl atoms in the NaCl structure. However, the corresponding unit cell (doubled along *c*) is greatly compressed along the *c* axis to an axial ratio $c/2a$ = 0.67. Otherwise, the transformation from the $I4_1/acd$ setting into the corresponding $F\ 4_1/d\ 1\ 2/c$ setting ($a' = a\sqrt{2}$ = 24.179 Å; $c' = c$ = 22.940 Å) immediately shows that the arrangement is really a subset of the supergroup $Fd\bar{3}c$ (No. 228), which includes 2^3 quasi *bcc* units cells of $Pn\bar{3}m$ symmetry (shaded in Figure 2b). Thus, it becomes obvious to look for relationships to the Cu_2O structure ($Pn\bar{3}m$ symmetry) with its two interpenetrating networks (β-cristobalite type).

Focusing our attention first on the tetrahedral anions, it can be recognised in Figure 3a that the Ba3 atoms connect the InP_4 tetrahedra forming a twisted 3D framework similar to that of β-cristobalite, where the Si atoms are replaced by InP_4 tetrahedra and the bridging O atoms are replaced by Ba3:

$$SiO_2 \triangleq [SiO_{4/2}] \triangleq [(InP_4)Ba_{4/2}]$$

A very important detail is the twisting of the network leading, with the given tetragonal symmetry, to a pair of interpenetrating structures with chiral sequences, that is both of them are three-dimensionally *meso* configured with alternating *R* and *S* segments (see Figure 4 and text below). This is not possible with tetrahedrally bonded nets under cubic symmetry.

As shown in Figure 5a, the two P1, the two P2 (corners of a InP_4 tetrahedron) and the two P3 form a P_6 octahedron around each Ba3 atom. These octahedra are condensed to fourfold screws $^{1}_{\infty}[Ba(P_4P_{2/2})]$ along [001] (black octahedra in Figure 2a).

Replacing the Ba3 atoms in Figure 3a by a whole BaP_6^{oct} octahedron, an equivalent framework is formed (Figure 3b), where now these octahedra play the role of bridging units. As illustrated in Figure 4, in $Ba_{14}InP_{11}$ there are two interpenetrating cristobalite-like frameworks (black and white *meso* configurations) of condensed InP_4 tetrahedra and BaP_6^{oct} octahedra *hierarchically* related to those in Cu_2O, where the O and Cu atoms are replaced by centred ($InP_{4/2}$) tetrahedra and ($BaP_4P_{2/2}$) octahedra, respectively:

$$[OCu_{4/2}][OCu_{4/2}] \triangleq [(InP_{4/2})(BaP_4P_{2/2})_{4/2}][(InP_{4/2})(BaP_4P_{2/2})_{4/2}]$$

However, it must be noticed that two corners of each P_6 octahedron (P1 in Figure 3c) are shared by both interpenetrating frameworks [not considered in the formula]. The remaining phosphorus atoms P4 are placed between two P1 atoms, forming the linear $[P_3]^{7-}$ units as illustrated in Figure 3c.

The concept of *hierarchy* between a simple and a complex structure was briefly introduced in ref.[17]. A complex structure is hierarchically related to a simple one, if each atom in the simple structure is replaced by an aggregate of atoms to generate the complex structure. The replacement can be partial or total. The polyhedral aggregates in the complex structures can be isolated, linked (present case) or might fill the space entirely. A more comprehensive work on hierarchical relationships is being prepared[18].

2.2.4 The Barium Building Units and Their Framework

As shown in Figure 3d, distorted Ba_8^{cub} cubes (second coordination sphere of Ba3) are formed when Ba1, Ba2 and

Figure 3. (a) One of the interpenetrating networks (β-cristobalite type) formed by tetrahedral $[InP_4]$ nodes and bridging Ba3 atoms. (b) Same as (a) but the Ba3 atoms were replaced by white BaP_6^{oct} octahedra (Ba3 is not shown). This twisted network is *meso* configured, containing alternately *R* and *S* fragments. (c) Detail of two neighbouring frameworks (shaded and black) showing an inserted P4 atom which form the centre of a $[P_3]$ triad. (d) Fragment of one network exhibiting the Ba_8^{cub} cubic frames around the BaP_6^{oct} octahedra

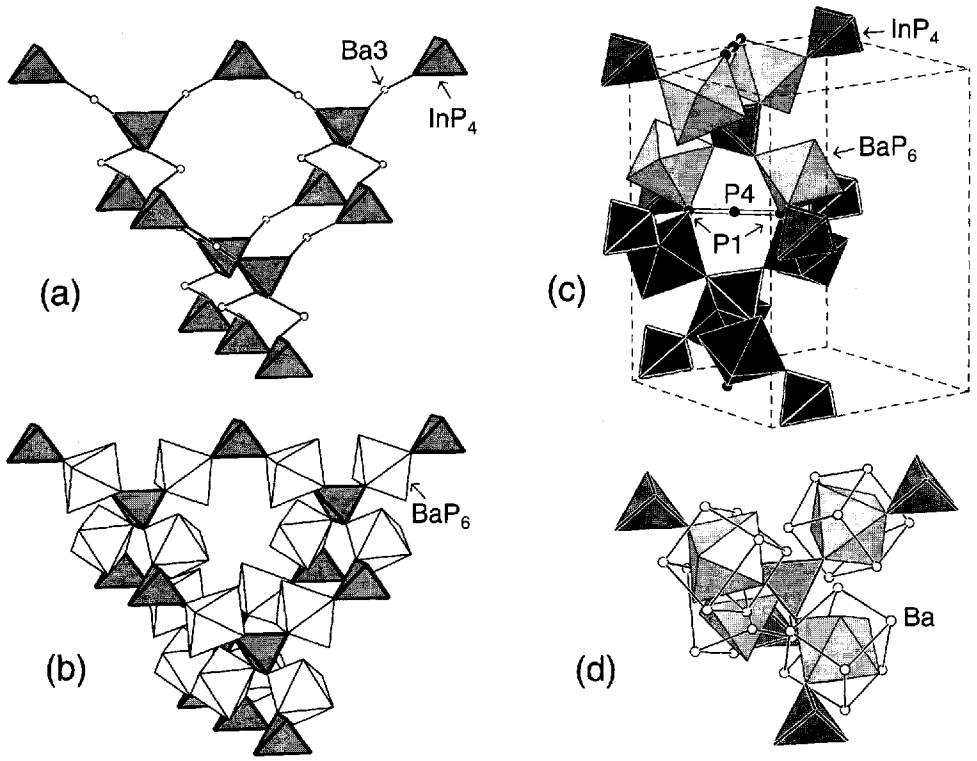

Figure 4. Stereopair of the two interpenetrating nets (white and black) in $Ba_{14}InP_{11}$, showing the hierachical framework of the Cu_2O-type. See Figure 3 and text for details

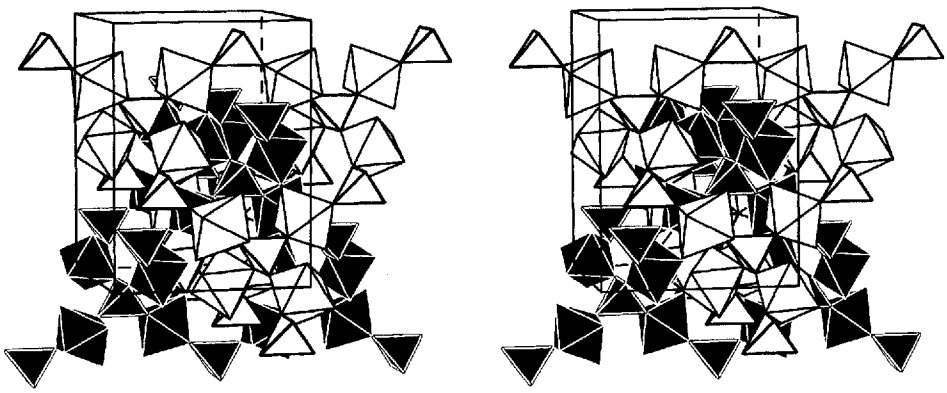

Ba4 atoms fill the voids of the phosphorus framework, capping the triangular faces of the BaP_6^{oct} octahedra (see also Figure 2a).

Let us now focus our attention on the Ba envelope of the $[P_3]^{7-}$ anion. Around P1 and P4 (atoms of the $[P_3]^{7-}$ unit) the Ba atoms build up bicapped Ba_8^{tp} trigonal prisms and Ba_8^{tap} tetragonal antiprisms, respectively (see Figure 1a). It can be seen in Figure 5b, that two pairs of edge-sharing $BaBa_8^{cub}$ cubes (centred by Ba3) and two PBa_6^{tp} trigonal prisms share rectangular faces with a central PBa_8^{tap} tetragonal antiprism, forming a twisted structural fragment (the P atoms around Ba3 cap the faces of the Ba_8^{cub} cubes). The packing of these fragments with their axial $[P_3]^{7-}$ segments perpendicular to the *c* axis in the (001) plane (adjacent segments are perpendicular to each other) results in an intergrowth of two equivalent but enantiomorphic 3D frameworks (R and S) of condensed $BaBa_8^{cub}$ cubes, PBa_8^{tp} trigonal prisms and PBa_8^{tap} tetragonal antiprisms (black and white in Figures 6 and 7). The holes between the frameworks are filled by $[InP_4]^{9-}$ tetrahedral units and P^{3-} anions (see also P3 in Figure 5c).

Inspection of the topology of the interpenetrating frameworks of the Ba polyhedra $Ba_{14}InP_{11}$ reveals a relationship to the framework of condensed $RhBi_{8/2}^{tap}$ tetragonal anti-

Figure 5. (a) The anionic octahedral environment of Ba3. (b), (c) Complementary details of the framework in Figures 6 and 7b, emphasising in (b) the axial skeletal network (formed by the atoms Ba3, P1 and P4) further connected to the $[InP_4]$ tetrahedra via P2 atoms (see also Figures 1a, 5a), and in (c) the distorted bicapped trigonal prism around P3 (P^{3-}) formed by the Ba atoms of one PBa_8^{tap} antiprism and one $BaBa_8^{cub}$ cube. (d) Polyhedra star of four bicapped trigonal prisms of metal atoms with one In atom as common corner at the centre (each prism is centred by P2).

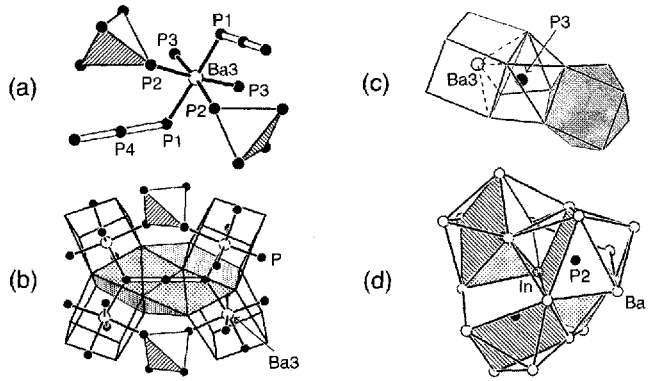

Figure 6. Fragments of the interpenetrating frameworks of edge- and face-sharing Ba polyhedra (black and white), namely PBa_6^{tp} trigonal prisms, PBa_8^{tap} tetragonal antiprisms and $BaBa_8^{cub}$ cubes (see also Figure 7b). The "interstitial" $[InP_4]$ tetrahedra (shaded) are also shown

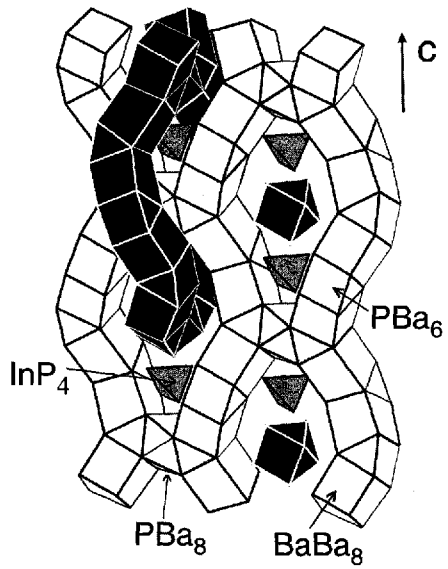

prisms in the cubic phase $RhBi_4$[19] as well as to the framework of the oxygen atoms in the garnet structure (space group $Ia\bar{3}d$). This is demonstrated in Figure 7. The coordination polyhedra $RhBi_{8/2}^{tap}$ are centred at the 24(*c*)sites. By connecting all 24(*c*) positions, the so-called V* network is formed, which consists of two interpenetrating enantiomorphic nets ^{+}V and ^{-}V. Also, the units around 24(*c*) act as "edges" of the so-called Y** network which is formed by the 16(*b*) site. In $RhBi_4$, the three-fold connected nodes of the Y** net are formed by empty Bi_6 trigonal prisms, which are connected by centred $RhBi_{8/2}^{tap}$ tetragonal antiprisms (Figure 7c). Indeed, $Ia\bar{3}d$ is also a supergroup of $I4_1/acd$. The symmetry reduction is here reflected in the replacement of a homogeneous V* graph of $RhBi_{8/2}^{tap}$ polyhedra by a heterogeneous V* graph of *one* centred $PBa_{8/2}^{tap}$ tetragonal antiprism and *two* centred $BaBa_8^{cub}$ cubes (Figures 6 and 7b). Here, the corresponding Y** nodes are formed by P-centred PBa_6 trigonal prisms. In more detail, this means that the "skeletal" V* network generated by the Rh 24(*c*) sites is replaced by a heterogeneous V* network generated by the P4 8(*b*) and Ba3 16(*e*) sites. The heterogeneous V* network in $Ba_{14}InP_{11}$ is shown in Figure 7a, where the two chiral nets are distinctly shaded (black and white).

Quantum mechanical calculations[19] have shown that in $RhBi_4$ the lone pairs of Bi atoms are located at the periphery of the $RhBi_8^{tap}$ polyhedra, forming hyperbolic layers. In this case, the periphery has Lewis base character. On the other hand, in $Ba_{14}InP_{11}$, the periphery of the Ba polyhedral frame has Lewis acid character, and the hyperbolic labyrinth between the two chiral graphs is filled by the basic units P^{3-} and $[InP_4]^{9-}$ (Figures 6 and 7).

It is interesting that the Ba atoms around the P (P2) ligands of the InP_4 anion form an unusual group of four condensed bicapped trigonal prisms (distorted), as demonstrated in Figure 4d.

As shown in Figure 1 (see also Table 2), the anisotropy in the displacement of the Ba atoms is most pronounced for Ba4. The displacement ellipsoid of Ba4 is elongated along one edge of the trigonal prism around P1. This displacement is obviously related to the orientational disorder of the $[P_3]^{7-}$ group ($[P-P\cdots P]$ or $[P\cdots P-P]$) changing the form and size of its Ba envelope.

2.3 Vibrational Spectra

In the $Ca_{14}AlSb_{11}$ structure type, the spectroscopically relevant units are the linear anions $[X-X-X]^{7-}$ and the tetrahedral metallate anions $[MX_4]^{9-}$. According to refs.[9,10], the $[X-X-X]^{7-}$ triads are more or less asymmetric. But in $Ba_{14}InP_{11}$, the $[P-P-P]^{7-}$ unit exhibits an exorbitantly asymmetry, corresponding to a $[P-P]^{4-}$ dumbbell weakly coupled to a P^{3-} anion (see section 2.1.2 and Figure 1e). In order to verify this feature and exclude other possibilities, e.g. a dynamic flip-flop motion of the central P4 atom, the Raman and IR spectra were recorded.

Both, the $[P-P]^{4-}$ dumbbell and the *symmetric* $[P-P-P]^{7-}$ linear polyanion belong to the point group $D_{\infty h}$, which give rise to one $[\Sigma_g(R)]$ and to three $[\Sigma_g(R), \Sigma_u(IR), \Pi_u(IR)]$ fundamentals, respectively, with $\Sigma_g(\nu_s)$ being the only Raman-active mode in each case. However, for a slightly *asymmetric* $[P-P-P]^{7-}$ unit (point group $C_{\infty v}$), the antisymmetric stretch (Σ_u) and bending (Π_u) vibrations also become Raman-active. But, these effects are weak and can overlap with the external modes.

In previous studies[18,19], it was found that the ratio of the values of the characteristic Raman frequencies for the isoelectronic pairs $Cl_2/[Cl_3]^-$ (539 cm^{-1}/268 cm^{-1} = 2.01) and $Br_2/[Br_3]^-$ (317 cm^{-1}/162 cm^{-1} = 1.96) is $\nu_1/\nu_2 \approx 2$. According to this, a similar $\nu_s(P-P)/\nu_s(P-P-P)$ ratio is also expected for the $[P-P]^{4-}$ dumbbell and the symmetric $[P-P-P]^{7-}$ unit, reflecting the differences in bond

Figure 7. Stereopairs: (a) The two interpenetrating enantiomorphic nets (black and white) of the heterogeneous V* network generated by the P4 atoms at 8*b* (shaded) and Ba3 atoms at 16*e* sites in $Ba_{14}InP_{11}$. Comparison of the two (black and white) interpenetrating enantiomorphic frameworks in the (b) tetragonal $Ba_{14}InP_{11}$ and (c) cubic $RhBi_4$ structures. In (c) the frameworks are only composed by condensed $RhBi_{8/2}^{tag}$ tetragonal antiprisms. In (b) the frameworks consists of condensed PBa_8^{tap} tetragonal antiprisms and $BaBa_8^{cub}$ cubes, the resulting Ba_8^{tp} trigonal prisms are filled by P1 atoms (which generate the Y** network, not shown). In $RhBi_4$ the Bi_6^{tp} prisms are empty. The "interstitial" InP_4 tetrahedra and P3 atoms (shaded) are also shown. Notice that the framework of the oxygen atoms in the garnet structure is equivalent to that of the bismuth atoms in the $RhBi_4$ structure. (See text for more details)

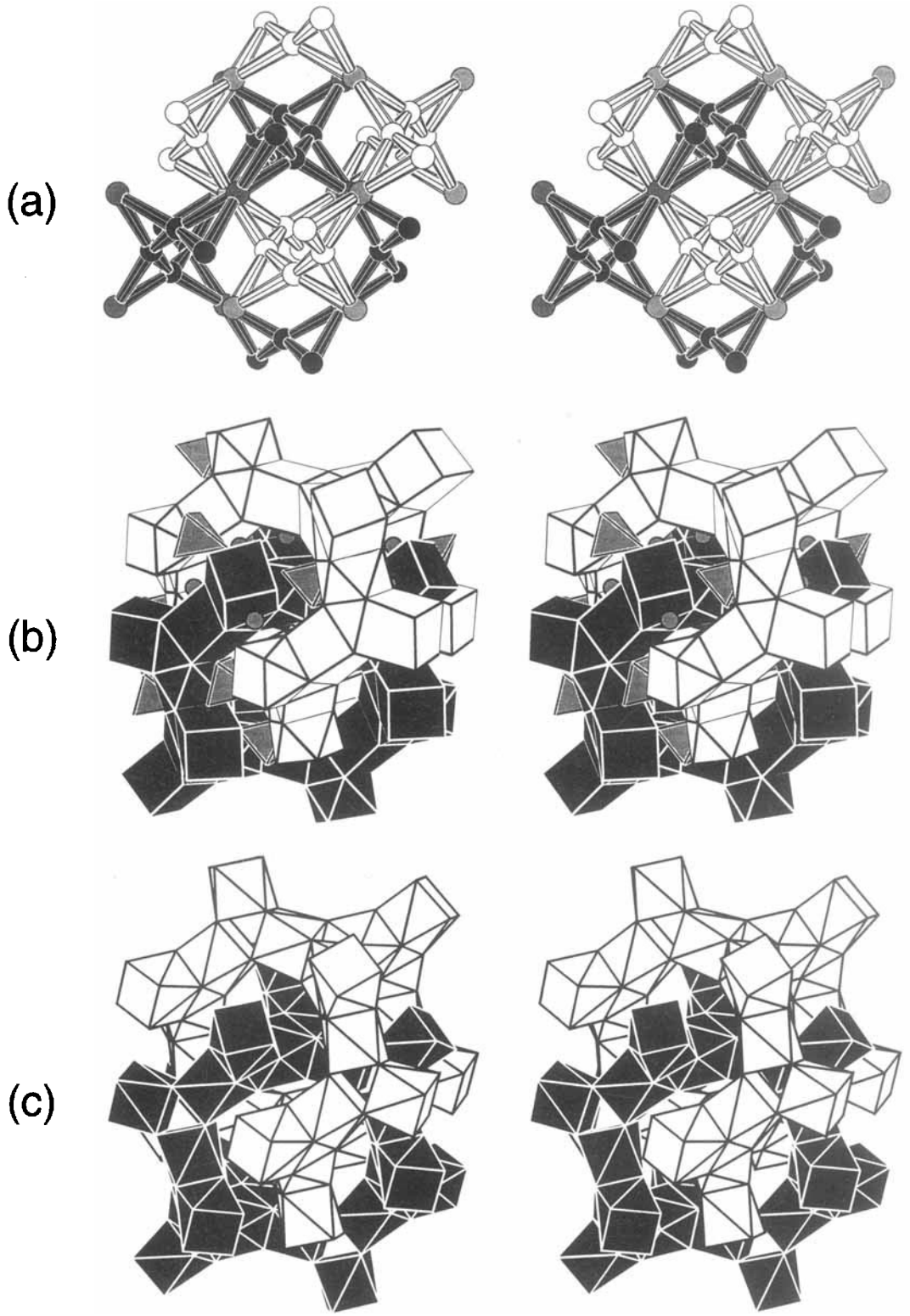

strengths. For a $[P-P-P]^{7-}$ polyanion with pronounced asymmetry, the ν_s value should be intermediate between those for a *symmetric* $[P-P-P]^{7-}$ triad and a $[P-P]^{4-}$ dumbbell, and in the case of a dynamic flip-flop motion of the central P atom, the characteristic band is expected to be rather broad.

Unfortunately, no spectral data of alkaline-earth metal compounds containing $[P-P]^{4-}$ dumbbells are available in the literature. Therefore, the Raman spectrum of Ba_5P_4 was also measured: $Ba_5P_4 \triangleq (Ba^{2+})_5([P_2]^{4-})(P^{3-})_2$[22]. The spectrum exhibits a characteristic P–P stretch at 355 cm^{-1}, which is considerably lower than ν_s(P–P) for P_2H_4 (436 cm^{-1})[23], reflecting the influence of the partial negative charge and the cationic environment of the P_2 dumbbells. Thus, a similar value of ν_s is also expected for the $[P-P]^{4-}$ unit in $Ba_{14}InP_{11}$.

Indeed, the Raman spectrum of $Ba_{14}InP_{11}$ (Figure 8b) shows a strong band at 324 cm^{-1}, which is absent in the corresponding IR spectrum (Figure 8a), and is assigned to a P–P stretch in accordance with the result for Ba_5P_4. The very strong Raman band at 237 cm^{-1} and the pair of bands at 252 cm^{-1} a 295 cm^{-1} (observed in the Raman and IR spectra with different intensities), are interpreted as the In–P stretches $\nu_1(A_1)$ and $\nu_3(F_2)$, respectively. The splitting of $\nu_3(F_2)$ is in good agreement with the site symmetry S_4 of the $[InP_4]^{9-}$ unit in the solid state. The remaining fundamentals, $\nu_2(E)$ and $\nu_4(F_2)$, are bending modes of the $[InP_4]^{9-}$ tetrahedron. Taking into account the vibrational data of the isoelectronic units $[InCl_4]^-$[24] and $SnCl_4$[20], they should appear below 120 cm^{-1} where the external modes dominate. Hence, no reasonable distinction between the external modes and the fundamentals $\nu_2(E)$ and $\nu_4(F_2)$ is possible in this frequency region.

Figure 8. (a) Raman and (b) infrared spectrum of $Ba_{14}InP_{11}$ at room temperature. The frequencies of the bands are indicated

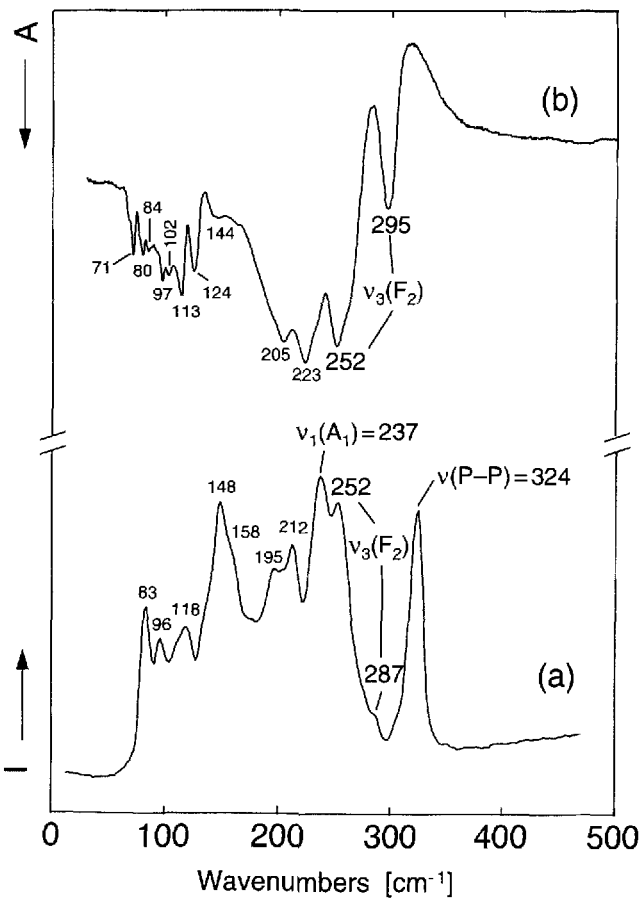

According to the results for Ba_5P_4, the external modes appear at frequencies lower than 230 cm^{-1}. Thus, in the spectrum of $Ba_{14}InP_{11}$ the two Raman bands at 212 cm^{-1} and 195 cm^{-1} and the strong IR bands at 223 cm^{-1} and 205 cm^{-1} are assigned to lattice vibrations in which the isolated P^{3-} anions mainly participated. In summary, the spectroscopic data clearly support the crystallographic analysis.

During the review process, we received a preprint[26] about $Ca_{14}GaP_{11}$ (second phosphide of this type) from J. D. Corbett. The asymmetry of the $[P_3]^{7-}$ triad in $Ca_{14}GaP_{11}$ is less pronounced ($d_1/d_2 = 0.75$) than in the present case ($d_1/d_2 = 0.56$), which also reflects the influence of the size of the cation cage that envelopes the triad[10].

We thank Prof. *W. Brockner* (TU Clausthal) for the recording of the IR and Raman Spectra and the *Fonds der Chemischen Industrie* for financial support.

Experimental

General: The starting materials as well as the products are sensitive to air and moisture; they were handled in an argon-filled glove box ($O_2 < 1$ ppm and $H_2O < 1$ ppm) that was equipped with a microscope. The barium metal used (3 N, Aldrich), was first distilled under high vacuum, and the red phosphorus (electr. grade, Hoechst, Knapsack) and InP (5N8, Aldrich) were used as purchased. The sealed stainless steel (or niobium) ampoules used for the reactions (diameter ϕ = 16 mm and length l = 80 mm) were heated in evacuated quartz tubes at 1345 K for 2–5 days and furnace cooled to room temp. over a 30 hour period. Typical batch sizes were 0.7–1.0 g. The X-ray powder diffraction patterns were recorded on a Stoe diffractometer. The optical diffuse reflection data of a powdered sample (filled in a sealed silica tube) was recorded with a Perkin Elmer Lambda 9 spectrometer.

X-ray Single-Crystal Data Collection: Single crystals of the title compound were isolated and sealed in glass capillaries. The X-ray diffraction data were measured on a Siemens-Nicolet four-circle diffractometer. The Laue symmetry and the systematic reflection absences were charcteristic of the space-group $I4_1/acd$ (No. 142). The lattice paramcters were determined from the least-squares refinement of the 2Θ values of 22 reflections with $10.7° < 2\Theta < 15.3°$. The crystallographic data are presented in Table 1.

Structure Analysis and Refinement: The lattice parameters and the space-group indicated a strong similarity to $Ca_{14}AlSb_{11}$ and to $Sr_{13}\square NbAs_{11}$[1,9]. The structure was refined using the full matrix, least-squares program SHELXTL-plus[25] with the positional parameters of $Ca_{14}AlSb_{11}$ as starting values. The first refinement converged to a conventional $F(F)$ value of 0.102, but the isotropic displacement parameter of the central P4 atom [8(*b*)site] of the P_3 unit was exorbitantly large (U_{iso} = 0.320; see Figure 1a), indicating either a large shift from the 8(*b*) site or a partial occupation of this site. An anisotropic refinement [$R(F)$ = 0.083] resulted in an highly elongated displacement ellipsoid which is oriented in the direction of the *exo*-atoms P1 along [110] (Figure 1b). Furthermore, the dif-

ference Fourier synthesis after a refinement without P4, showed a peak at the 16(f) position about 0.7 Å distant from the 8*b* site. The split model refinement (60 refined parameters) converged to a $R(F)$ value of 0.080 and gave a reasonable isotropic displacement parameter for P4 (Figure 1c, Table 2). Moreover, the *exo*-atom P1 also shows an elongated displacement ellipsoid (Figure 1c) oriented along [110]. From the values U_{11}, U_{22} and U_{12} (Table 2) follows that this feature corresponds to a splitting of the average 16(*f*) position into two 16(*f*) sites (about 0.35 Å apart) with 50% occupation probability. The final refinement with P1 in two independent 16(*f*) split sites, P11 and P12 (both with occupancy 0.50), resulted in a normal isotropic displacement parameters (reset) for both positions. The residual $R(F)$ value (58 refined parameters) was unchanged, but two less parameters were refined.

The final refined positional and displacement parameters are presented in Table 2. The main interatomic distances and angles are given in Table 3. Figure 1 shows the systematically varying stages in the refinement of the $[P_3]^{7-}$ anion[27].

Spectroscopic Measurements: The room temperatures Raman spectrum was recorded with a Raman module FRA 106 (Nd: YAG-Laser, 1.064 nm, 200 mW) attached to a Bruker IFS 66v spectrometer. The sample used was a powder of selected crystals of $Ba_{14}InP_{11}$ sealed in a silica tube. The infrared transmission spectrum was obtained from $Ba_{14}InP_{11}$–PE pellets with a Bruker IFS 66v spectrometer.

[1] G. Cordier, H. Schäfer, M. Stelter, *Z. Anorg. Allg. Chem.* **1984**, *519*, 183–188.
[2] K. F. Tebbe in *Homoatomic Rings, Chains and Macromolecules of Main-Group Elements.* (Ed.: A. L. Rheingold), Amsterdam, **1977**, chapter 24.
[3] S. M. Kauzlarich, M. M. Thomas, D. A. Odink, M. M. Olmstead, *J. Amer. Chem. Soc.* **1991**, *113*, 7205–7208.
[4] S. L. Brock, L. J. Weston, M. M. Olmestead, S. M. Kauzlarich, *J. Solid State Chem.* **1993**, *107*, 513–523.
[5] A. Rehr, S. M. Kauzlarich, *J. Alloys Comp.* **1994**, *207/208*, 424–462.
[6] T. Y. Kuromoto, S. M. Kauzlarich, D. J. Webb, *Chem. Mater.* **1992**, *4*, 435–440.
[7] D. P. Siemens, J. Del Castillo, W. Potter, D. J. Webb, T. Y. Kurumoto, S. M. Kauzlarich, *Solid State Commun.* **1992**, *84*, 1029–1031.
[8] J. Del Castillo, W. Potter, D. J. Webb, S. M. Kauzlarich, T. Y. Kurumoto, *Phys. Rev.* **1993**, *B47*, 4849–4852.
[9] K. Vidyasagar, W. Hönle, H. G. von Schnering, *Z. Anorg. Allg. Chem.* **1996**, *622*, 518–524.
[10] H. G. von Schnering, W. Hönle, in preparation.
[11] K. G. Mass, *Z. anorg. allg. Chem.* **1970**, *374*, 11–18.
[12] G. Cordier, E. Czech, M. Jakowski, H. Schäfer, *Rev. Chim. Minér.* **1981**, *18*, 9–18.
[13] H. Schäfer, *J. Solid State Chem.* **1985**, *57*, 97–111.
[14] R. Nesper, *Prog. Solid State Chem.* **1990**, *20*, 1–43.
[15] H. G. von Schnering, W. Hönle, *Chem. Rev.* **1988**, *88*, 243–273.
[16] G. Donnay, R. Allmann, *Am. Mineral.* **1970**, *55*, 1003–1015; R. Allmann, *Monatsh. Chem.* **1975**, *106*, 779–793.
[17] W. Carrillo-Cabrera, N. Caroca-Canales, H. G. von Schnering, *Z. anorg. allg. Chem.* **1994**, *14*, 247–257.
[18] H. G. von Schnering, W. Carrillo-Cabrera, in preparation.
[19] Y. Grin, U. Wedig, H. G. von Schnering, *Angew. Chem.* **1995**, *107*, 1318–1320; *Angew. Chem. Int. Ed. Engl.* **1995**, *34*, 1204–1206.
[20] J. Weidlein, U. Müller, K. Dehnicke in *Schwingungsfrequenzen I*, Georg Thieme Verlag, Stuttgart, **1981**, pp. 31, 48.
[21] W. Gabes, H. Gerding, *J. Mol. Struct.* **1972**, *14*, 267–269.
[22] H.-U. Terschüren, Thesis, Universität Kiel, **1989**.
[23] J. D. Odom, C. J. Wurrey, L. A. Carreira, J. R. Durig, *Inorg. Chem.* **1975**, *14*, 2849–2853.
[24] J. G. Contreras, D. G. Tuck, *Inorg. Chem.* **1972**, *11*, 2967–2971.
[25] G. M. Sheldrick, *SHELXTL PLUS, Release 4.0 Program for Solving, Refining and Displaying Crystal Structures*, Siemens Analytical X-Ray Instruments, **1990**.
[26] J. T. Vaughey, J. D. Corbett, *Chem. Mater.* **1996**, *8*, 671–675.
[27] Further details of the crystal structure investigation are available from the Fachinformationszentrum Karlsruhe, D-76344 Eggenstein-Leopoldshafen (Germany), on quoting the depository number CSD-405398.

[96088]